

The colour–magnitude relation of elliptical and lenticular galaxies in the ESO Distant Cluster Survey

Yara L. Jaffé,^{1,2*} Alfonso Aragón-Salamanca,¹ Gabriella De Lucia,³ Pascale Jablonka,⁴ Gregory Rudnick,⁵ Roberto Saglia^{6,7} and Dennis Zaritsky⁸

¹*School of Physics and Astronomy, University of Nottingham, University Park, Nottingham NG7 2RD*

²*European Southern Observatory, Karl-Schwarzschild Strasse 2, 85748 Garching, Germany*

³*Osservatorio Astronomico di Trieste INAF, Via Tiepolo 11, 34143 Trieste, Italy*

⁴*Laboratoire d'Astrophysique, Ecole Polytechnique Fédérale de Lausanne (EPFL), CH-1290 Sauverny, Switzerland*

⁵*Department of Physics and Astronomy, University of Kansas, 1251 Wescoe Hall Dr., Lawrence, KS 66045-7582, USA*

⁶*Max Planck Institut für extraterrestrische Physik, Giessenbachstrasse, 85748 Garching, Germany*

⁷*Universitätssternwarte, Scheinerstrasse 1, 81679 München, Germany*

⁸*Steward Observatory, University of Arizona, 933 North Cherry Avenue, Tucson, AZ 85721, USA*

Accepted 2010 July 27. Received 2010 July 7; in original form 2010 March 23

ABSTRACT

In this paper we study the colour–magnitude relation (CMR) for a sample of 172 morphologically classified elliptical and S0 cluster galaxies from the ESO Distant Cluster Survey (EDisCS) at $0.4 \lesssim z \lesssim 0.8$. The intrinsic colour scatter about the CMR is very small ($\langle \sigma_{\text{int}} \rangle = 0.076$) in rest-frame $U - V$. However, there is a small minority of faint early-type galaxies (7 per cent) that are significantly bluer than the CMR. We observe no significant dependence of σ_{int} with redshift or cluster velocity dispersion. Because our sample is strictly morphologically selected, this implies that by the time cluster elliptical and S0 galaxies achieve their morphology, the vast majority have already joined the red sequence. The only exception seems to be the very small fraction of faint blue early types. Assuming that the intrinsic colour scatter is due to differences in stellar population ages, we estimate the galaxy formation redshift z_{F} of each cluster and find that z_{F} does not depend on the cluster velocity dispersion. However, z_{F} increases weakly with cluster redshift within the EDisCS sample. This trend becomes very clear when higher redshift clusters from the literature are included. This suggests that, at any given redshift, in order to have a population of fully formed ellipticals and S0s they needed to have formed most of their stars $\simeq 2\text{--}4$ Gyr prior to observation. That does not mean that *all* early-type galaxies in *all* clusters formed at these high redshifts. It means that the ones we see already having early-type morphologies also have reasonably old stellar populations. This is partly a manifestation of the ‘progenitor bias’, but also a consequence of the fact that the vast majority of the early-type galaxies in clusters (in particular the massive galaxies) were already red (i.e. already had old stellar populations) by the time they achieved their morphology. Elliptical and S0 galaxies exhibit very similar colour scatter, implying similar stellar population ages. The scarcity of blue S0s indicates that, if they are the descendants of spirals whose star formation has ceased, the parent galaxies were already red when they became S0s. This suggests the red spirals found preferentially in dense environments could be the progenitors of these S0s. We also find that fainter early-type galaxies finished forming their stars later (i.e. have smaller z_{F}), consistent with the cluster red sequence being built over time and the brightest galaxies reaching the red sequence earlier than fainter ones. Combining the CMR scatter analysis with the observed evolution in the CMR zero-point we find that the early-type cluster galaxy population must have had their star formation truncated/stopped over an extended period $\Delta t \gtrsim 1$ Gyr.

Key words: galaxies: clusters: general – galaxies: elliptical and lenticular – galaxies: evolution.

*E-mail: ppxyj@nottingham.ac.uk

1 INTRODUCTION

Galaxy clusters have proven to be very useful laboratories for the study of galaxy formation and evolution. They can provide large and diverse galaxy samples across practically small areas of sky. Although the relative importance of nature and nurture in shaping galaxy evolution remains debated, it is well established that many galaxy properties in the nearby Universe correlate strongly with their environment. In particular, Postman & Geller (1984) and Dressler (1980) found that the morphological mix changes as a function of local galaxy density, with early-type galaxies (E/S0) dominating in locally dense environments, while late types (spirals and irregular galaxies) become increasingly important towards lower densities. Moreover, at low redshift there is an obvious bimodality in the colours of cluster galaxies that is well correlated with morphology (e.g. see recent work by Conselice 2006; Wang et al. 2007). The ‘blue cloud’ is dominated by spirals and irregular galaxies, and the prominent ridge of red galaxies (the so-called ‘red sequence’) is mainly populated by E/S0 galaxies. This implies that morphology correlates at some level with the stellar population content (and hence colour).

Baum (1959), Faber (1973) and Caldwell (1983) established the existence of a red sequence of cluster ellipticals in the local Universe and showed that these galaxies have systematically redder colours with increasing luminosity. Visvanathan & Sandage (1977) and Sandage & Visvanathan (1978a,b) found that this colour–magnitude relation (CMR) is universal. The detailed study of the *UVK* colours of local cluster early-type galaxies carried out by Bower, Lucey & Ellis (1992) confirmed Sandage & Visvanathan’s anticipation that both S0s and ellipticals follow the same relation. Furthermore, they also showed that the observed scatter about the CMR is very small (~ 0.04 mag in $U - V$ for their sample).

In the past decade, a number of studies have shown that the CMR of elliptical galaxies holds at progressively higher redshifts, at least up to $z = 1.4$ (e.g. Ellis et al. 1997; Stanford, Eisenhardt & Dickinson 1998; van Dokkum et al. 2000, 2001; Blakeslee et al. 2003; Mei et al. 2006; Lidman et al. 2008). As a consequence, the CMR is, arguably, one of the most powerful scaling relations obeyed by the early-type galaxy population at the cores of clusters, encoding important information about their formation history.

The slope of the CMR has traditionally been interpreted as the direct consequence of a mass–metallicity relation (e.g. Faber 1973; Larson 1974; Gallazzi et al. 2006). The classical explanation of this mass–metallicity sequence is based on the idea that star-formation-induced galactic outflows would be more efficient at expelling metal-enriched gas in low-mass galaxies than in massive ones (e.g. Larson 1974; Dekel & Silk 1986; Arimoto & Yoshii 1987; De Lucia, Kauffman & White 2004a; Tremonti et al. 2004; Kobayashi, Springel & White 2007; Finlator & Davé 2008). An alternative interpretation in which the CMR is predominantly an age sequence would imply that the relation changes significantly with redshift as less massive galaxies approach their formation epochs. The possibility that age is the main driver for the CMR was ruled out by observations of clusters at intermediate redshift that showed that the slope of the CMR evolves little with redshift (Kodama & Arimoto 1997; Kodama et al. 1998). Nevertheless, weak age trends along the CMR have been claimed (e.g. Ferreras, Charlot & Silk 1999; Poggianti et al. 2001; Nelan et al. 2005), even though it seems clear that they are not the main physical driver.

Bower et al. (1992) interpreted the small scatter about the CMR as the result of small age differences at a given galaxy mass. The

tightness of the relation then implies very synchronized star formation histories for these galaxies. Larger colour scatter would imply later episodes of star formation, or a wider range in galaxy formation redshifts. These results are not only indicative of the passive evolution of elliptical galaxies but also of an early formation epoch ($z > 2-3$; e.g. Bower et al. 1992; Blakeslee et al. 2003; Mei et al. 2009). Studies of absorption-line indices in the spectra of early-type galaxies also imply old ages (e.g. Trager et al. 1998). Some evidence has been found that the mean stellar ages of early-type galaxies may depend on their stellar mass in the sense that lower mass galaxies appear to have formed their stars at later epochs than the more massive ones (e.g. Thomas et al. 2005), although Trager, Faber & Dressler (2008) find no such trend in their study of the Coma cluster.

The above interpretation of the nature of the CMR, although traditionally accepted, has an important problem: it assumes that all red-sequence galaxies that we see today can be identified as red-sequence members of high-redshift galaxy clusters. As noted by van Dokkum & Franx (1996), this assumption is probably wrong because of the so-called *progenitor bias*: if the progenitors of some early-type galaxies were spirals at higher redshift, they would not be included in the higher redshift samples, which biases the studied population towards older ages. This effect has been corroborated by recent studies of the CMR evolution. De Lucia et al. (2007) found a significant deficit of faint red cluster galaxies at $0.4 \lesssim z \lesssim 0.8$ compared to galaxy clusters in the local Universe. They conclude that the red-sequence population of high-redshift clusters does not contain all the progenitors of nearby red-sequence cluster galaxies (see also De Lucia et al. 2009, and references therein). Tanaka et al. (1998) also find such deficit in a galaxy cluster at $z = 1.1$. We will come back to this issue in Sections 4 and 7.

In this paper, we study the CMR for a total sample of 174 morphologically selected elliptical and S0 galaxies contained in 13 galaxy clusters and groups at $0.4 \lesssim z \lesssim 0.8$ from the ESO Distant Cluster Survey (EDisCS; White et al. 2005), taking advantage of the availability of extensive *Hubble Space Telescope* (*HST*) imaging obtained with the Advanced Camera for Surveys (ACS) and extensive ground-based imaging and spectroscopy (see Section 2). We interpret the scatter about the CMR as a proxy for age (or formation time t_F), and study its dependence on intrinsic galaxy properties such as their luminosities and morphologies, and the role of the environment as quantified by the mass/velocity dispersion of the clusters. We complement the scatter analysis with information derived from the zero-point of each cluster’s CMR to constrain not only the formation epoch of early-type galaxies but also the duration of their formation phase.

It is important to point out that, even though there is much evidence suggesting that the CMR scatter is principally driven by galaxy age (e.g. Kodama & Arimoto 1997; Kauffmann & Charlot 1998; Bernardi et al. 2005), metallicity variations could also contribute to it (Nelan et al. 2005). If that is the case, the stellar ages we derive in this paper would be lower limits since the colour scatter we measure would contain both an age component and a metallicity one. Taking the results of Nelan et al. (2005) at face value, the maximum scatter in metallicity at a given velocity dispersion (luminosity) is ~ 0.1 dex, implying that at most we could be systematically underestimating the stellar ages by ~ 0.15 dex, where we have assumed Worthey (1994) 3/2 age–metallicity degeneracy law. Notwithstanding this caveat, even if the absolute ages were affected at this level, it is not unreasonable to expect that the effect on relative ages (the main focus of this paper) would be smaller.

This paper is organized as follows: our data set and the sample of early-type galaxies are described in Section 2. In Section 3, we explain the ‘scatter–age method’ used in this work to study the formation histories of early-type galaxies. Section 4 shows the scatter measured about the CMRs, Section 5 the results of the scatter–age test and Section 6 the zero-point analysis. Finally, we discuss our results and draw conclusions in Section 7.

Throughout this work, we use Vega magnitudes and adopt a *Wilkinson Microwave Anisotropy Probe* (*WMAP*) cosmology (Spergel et al. 2007) with $\Omega_M = 0.28$, $\Omega_\Lambda = 0.72$ and $H_0 = 70 \text{ km s}^{-1} \text{ Mpc}^{-1}$.

2 THE DATA

EDisCS originated as an ESO Large Programme designed to study cluster structure and cluster galaxy evolution over a large fraction of cosmic time (White et al. 2005). The complete data set consists of 20 fields containing galaxy clusters at redshifts between 0.4 and 1. The sample was constructed selecting 30 of the highest surface brightness candidates in the Las Campanas Distant Cluster Survey (Gonzalez et al. 2001), and confirming the presence of an apparent cluster and a possible red sequence with Very Large Telescope (VLT) 20-min exposures in two filters. From these candidates, 10 of the highest surface brightness clusters were followed up in each of two bins at estimated redshifts $0.45 < z_{\text{est}} < 0.55$ and $0.75 < z_{\text{est}} < 0.85$, where z_{est} was based on the magnitude of the putative brightest cluster galaxy.

For the 20 fields with confirmed cluster candidates, deep optical imaging was taken using the Focal Reducer/low dispersion Spectrograph 2 (FORs2) camera and spectrograph at the VLT. A full description of the available optical images and photometry is given in White et al. (2005). In brief, the optical photometry consists of *B*, *V* and *I* imaging for the 10 intermediate-redshift ($z_{\text{est}} \simeq 0.5$) cluster candidates and *V*, *R* and *I* imaging for the 10 high-redshift ($z_{\text{est}} \simeq 0.75$) cluster candidates. Typically, the integration times were 45 min for the intermediate-redshift sample and 2 h for the high-redshift sample. In addition, near-infrared (IR) *J* and *K* photometry was obtained using the Son of ISAAC (SofI) camera at the New Technology Telescope (NTT; Aragón-Salamanca et al., in preparation). This was obtained for all but three fields, two of them were rejected due to bad weather and an additional field was rejected because its spectroscopic redshift histogram was not cluster like. FORs2 at the VLT was also used to obtain multi-object spectroscopy for ~ 100 objects in each field (see Halliday et al. 2004; Milvang-Jensen et al. 2008). The redshift data were used to confirm the physical reality of the clusters and measure their velocity dispersions. This process revealed that several of the fields contained multiple clusters and groups at different redshifts (Halliday et al. 2004; Poggianti et al. 2006; Milvang-Jensen et al. 2008). Additional follow-up includes narrow-band $H\alpha$ imaging (Finn et al. 2005) and XMM X-ray observations (Johnson et al. 2006) for a subset of the clusters. Moreover, 10 of the highest redshift clusters in the sample were also imaged with *HST*’s ACS camera in the *F814W* filter, from which reliable visual morphologies were derived for a large sample of cluster and field galaxies (see Desai et al. 2007, for details).

For consistency with our previous work on the CMR of EDisCS cluster galaxies (De Lucia et al. 2007), in the following we use magnitudes and colours measured in seeing-matched images with full width at half-maximum (FWHM) = 0.8 arcsec (the typical seeing in the optical images), using a fixed 1.0 arcsec radius circular aperture. This aperture represents a compromise between minimizing sky-subtraction and contamination errors and being as close

as possible to measuring global colours. We note that 1.0 arcsec corresponds to $\simeq 7 \text{ kpc}$ at $z \simeq 0.7$, and at these redshifts early-type galaxies in the luminosity range considered here have half-light radii $\sim 3 \text{ kpc}$ (Treu et al. 2005; Trujillo et al. 2007). The associated photometric errors were derived by placing empty apertures in regions of the image without detected objects to estimate accurately the sky contribution to the error budget. This is justified since the sky noise is the dominant source of error when measuring the aperture magnitudes of our faint galaxies (see White et al. 2005, for details).

In this paper, we focus on a subsample of the EDisCS data set consisting of 174 galaxies in 13 clusters and groups. This selection was based on the following criteria.

(i) The galaxies must be spectroscopically confirmed cluster/group members (Halliday et al. 2004; Milvang-Jensen et al. 2008). This ensures a very clean sample, avoiding the uncertainties introduced by other cluster membership criteria such as photometric redshifts (Pello et al. 2009; Rudnick et al. 2009). The penalty is, of course, a significant reduction in the sample size.

(ii) They must have early-type morphology (E or S0), based on visual classification from *HST* images (Desai et al. 2007). We note that by imposing this, the sample reduces to galaxies within the 10 fields observed with *HST*.

(iii) The galaxies should belong to clusters/groups with at least four early-type members in order to measure the CMR scatter with reasonable accuracy. This allows us to detect the presence of an intrinsic colour scatter with $> 3\sigma$ confidence in all cases.

Since all spectroscopically confirmed members in the *HST*-covered area have been morphologically classified, the selection function of our sample is the same as that of the spectroscopic sample. This means that for all practical purposes our early-type galaxy sample behaves like the original *I*-band selected spectroscopic sample (Milvang-Jensen et al. 2008), and therefore as a rest-frame *B*-band selected sample. On average we typically reach $M_B < -18.5$, with some cluster-to-cluster variation. Although all our analysis has been carried out using this empirically defined *I*-band selected sample, thus maximizing the sample size, we have checked that using a rest-frame *B*-band luminosity selected sample would not have altered any of our conclusions. We have also checked that the spectroscopic selection function does not affect our conclusions. We produced Monte Carlo realizations of the colour–magnitude diagram (CMD) of our sample taking into account the empirical selection function determined by Milvang-Jensen et al. (2008) and found that the simulated colour scatter agrees very well with the measured one.

To test the robustness of the morphologies for the galaxies in our sample, we re-examined visually their *HST* images (see Fig. 1) and found only two galaxies that had been misclassified as early types in Desai et al. (2007). The first one, EDCSN J1138096–1135223, is clearly not an elliptical and shows a very perturbed morphology. The second one, EDCSN J1138127–1134190, is in a dense group of (probably) interacting galaxies and there is a brighter elliptical very close to the position of this object. It is obvious that the wrong galaxy was classified. The last two lines of Table 4 show some of the properties of these two galaxies and their *HST F814W* images are shown in the bottom row of Fig. 1. It is not surprising that both galaxies are substantially bluer than the red sequence. They are also quite faint, where visual classification is, perforce, less reliable. These two misclassified galaxies were removed from our sample and will not be discussed further. We noticed that six out of the remaining 172 galaxies (3.5 per cent) have signs of perturbation,

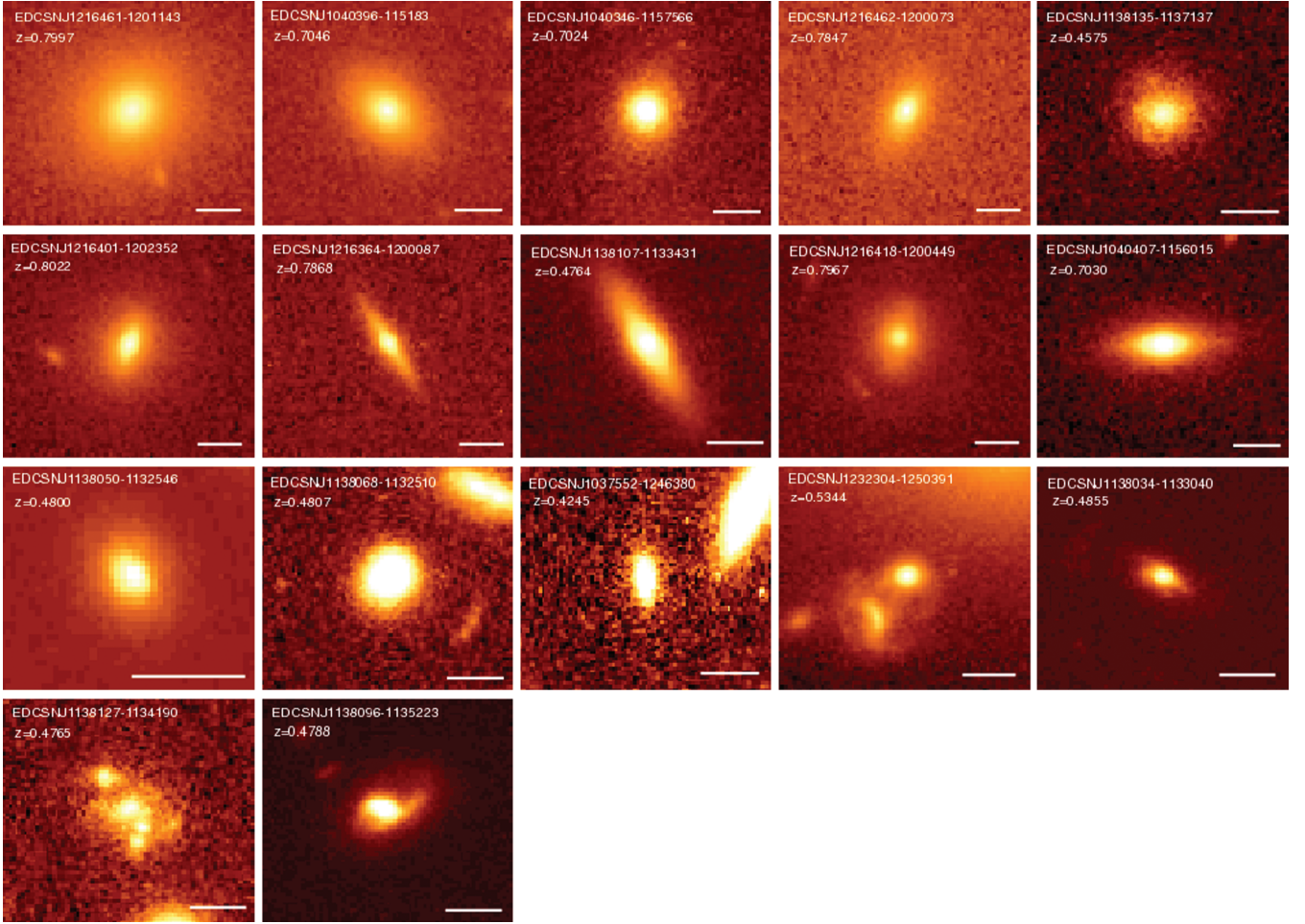


Figure 1. *HST F814W* images for a representative sample of ellipticals (top row), S0s (second row) and ‘blue tail’ galaxies (third row). The last row shows the two galaxies that were excluded from our study due to morphological misclassification. The rightmost two galaxies in the third row (blue tail) exhibit some degree of perturbation in their morphologies (see text for further discussion). The horizontal white lines correspond to 5 kpc.

although their early-type morphology is clear. Interestingly, two out of these six slightly perturbed galaxies are significantly bluer than the CMR. We will come back to this in Section 4.

The cluster sample with the corresponding redshifts, line-of-sight velocity dispersions (σ_v) and number of early-type members is shown in Table 1. The σ_v s are taken from Halliday et al. (2004) and Milvang-Jensen et al. (2008). The reliability of these velocity dispersions as mass estimators has been confirmed by weak lensing (Clowe et al. 2006) and X-ray (Johnson et al. 2006) estimates.

3 METHOD: THE SCATTER-AGE TEST

The scatter-age test carried out in this paper was developed by Bower et al. (1992) as a reasonably simple, yet powerful method for constraining the formation history of early-type galaxies. They applied it at $z \sim 0$ to galaxies in the Virgo and Coma clusters. Ellis et al. (1997) applied the same test to galaxies in three $z \sim 0.54$ clusters. We apply it here to a much larger cluster sample, covering a significant cluster mass range. We have the added advantage that since 1997 the uncertainty in the cosmological parameters, and thus the transformation of redshift into look-back time, has decreased considerably. We also benefit from a large and homogeneous galaxy sample in a wide range of redshift and cluster velocity dispersion

Table 1. Properties of the cluster sample. The columns correspond to cluster ID, spectroscopic redshift, line-of-sight velocity dispersion, number (N) of early-type galaxies (E+S0), number ellipticals ($N(E)$) taken into account in the scatter calculation and number of ‘blue tail’ members (N_{blue}). See text for details. Cluster redshifts and velocity dispersions were taken from Halliday et al. (2004) and Milvang-Jensen et al. (2008).

| Cluster name | z | σ_v (km s $^{-1}$) | $N(\text{E+S0})$ | $N(\text{E})$ | N_{blue} |
|-----------------|--------|----------------------------|------------------|---------------|-------------------|
| CL 1037.9–1243a | 0.4252 | 537^{+46}_{-48} | 12 | 7 | 1 |
| CL 1138.2–1133a | 0.4548 | 542^{+63}_{-71} | 9 | 7 | 1 |
| CL 1138.2–1133 | 0.4796 | 732^{+72}_{-76} | 16 | 11 | 3 |
| CL 1232.5–1250 | 0.5414 | 1080^{+119}_{-89} | 23 | 15 | 3 |
| CL 1354.2–1230a | 0.5952 | 433^{+95}_{-104} | 4 | 4 | 0 |
| CL 1103.7–1245a | 0.6261 | 336^{+36}_{-40} | 4 | 4 | 0 |
| CL 1227.9–1138 | 0.6357 | 574^{+72}_{-75} | 8 | 3 | 0 |
| CL 1054.4–1146 | 0.6972 | 589^{+78}_{-70} | 16 | 14 | 2 |
| CL 1040.7–1155 | 0.7043 | 418^{+55}_{-46} | 8 | 7 | 0 |
| CL 1054.7–1245a | 0.7305 | 182^{+58}_{-69} | 6 | 5 | 0 |
| CL 1054.7–1245 | 0.7498 | 504^{+113}_{-65} | 18 | 13 | 0 |
| CL 1354.2–1230 | 0.7620 | 648^{+105}_{-110} | 5 | 4 | 2 |
| CL 1216.8–1201 | 0.7943 | 1018^{+73}_{-77} | 31 | 18 | 0 |

Table 2. Values of the measured intrinsic scatter (σ_{int}) and the calculated formation time (t_{F}) and redshift (z_{F}) for solar metallicity and $\beta = 0.1, 0.3$ and 1.0 . The associated uncertainties correspond to the random errors (16 and 84 per cent confidence levels in a χ^2 distribution). Recall that t_{F} is the look-back time, from the cluster redshift, since star formation ceased.

| Cluster name | z | CMR colour | σ_{int} | $t_{\text{F}}(\beta = 0.1)$ (Gyr) | $t_{\text{F}}(\beta = 0.3)$ (Gyr) | $t_{\text{F}}(\beta = 1.0)$ (Gyr) | $z_{\text{F}}(\beta = 0.1)$ | $z_{\text{F}}(\beta = 0.3)$ | $z_{\text{F}}(\beta = 1.0)$ |
|-----------------|--------|------------|---------------------------|--------------------------------------|--------------------------------------|--------------------------------------|-----------------------------|-----------------------------|-----------------------------|
| CL 1037.9–1243a | 0.4252 | $V - I$ | $0.09^{+0.03}_{-0.01}$ | $2.3^{+0.4}_{-0.6}$ | $4.4^{+0.3}_{-0.4}$ | $6.0^{+0.2}_{-0.3}$ | $0.76^{+0.08}_{-0.1}$ | 1.3 ± 0.1 | $2.1^{+0.1}_{-0.2}$ |
| CL 1138.2–1133a | 0.4548 | $V - I$ | $0.10^{+0.03}_{-0.02}$ | $2.4^{+0.2}_{-0.3}$ | $3.34^{+0.1}_{-0.2}$ | $4.0^{+0.1}_{-0.1}$ | $0.82^{+0.04}_{-0.06}$ | $1.03^{+0.03}_{-0.05}$ | 1.22 ± 0.03 |
| CL 1138.2–1133 | 0.4796 | $V - I$ | $0.09^{+0.03}_{-0.01}$ | $2.1^{+0.3}_{-0.4}$ | $3.7^{+0.2}_{-0.3}$ | $5.1^{+0.2}_{-0.3}$ | $0.79^{+0.06}_{-0.07}$ | $1.19^{+0.07}_{-0.09}$ | 1.8 ± 0.1 |
| CL 1232.8–1201 | 0.5414 | $R - I$ | $0.08^{+0.02}_{-0.01}$ | $1.8^{+0.3}_{-0.4}$ | $3.8^{+0.2}_{-0.3}$ | $5.1^{+0.2}_{-0.3}$ | $0.82^{+0.06}_{-0.07}$ | $1.40^{+0.008}_{-0.1}$ | 2.6 ± 0.2 |
| CL 1354.2–1230a | 0.5952 | $R - I$ | $0.04^{+0.03}_{-0.009}$ | $2.2^{+0.5}_{-1}$ | $4.2^{+0.4}_{-1}$ | $5.7^{+0.3}_{-0.7}$ | $1.0^{+0.1}_{-0.3}$ | $1.7^{+0.2}_{-0.4}$ | $2.8^{+0.3}_{-0.6}$ |
| CL 1103.7–1245a | 0.6261 | $R - I$ | $0.08^{+0.07}_{-0.02}$ | $1.0^{+0.6}_{-0.9}$ | $3.1^{+0.4}_{-1}$ | $4.7^{+0.3}_{-0.8}$ | $0.8^{+0.1}_{-0.2}$ | $1.4^{+0.2}_{-0.4}$ | $2.2^{+0.2}_{-0.5}$ |
| CL 1227.9–1138 | 0.6357 | $R - I$ | $0.09^{+0.04}_{-0.02}$ | $0.5^{+0.4}_{-0.4}$ | $2.5^{+0.3}_{-0.6}$ | $4.1^{+0.2}_{-0.4}$ | $0.71^{+0.07}_{-0.06}$ | $1.2^{+0.1}_{-0.2}$ | $1.8^{+0.1}_{-0.2}$ |
| CL 1054.4–1146 | 0.6972 | $R - I$ | $0.06^{+0.02}_{-0.01}$ | $1.0^{+0.3}_{-0.5}$ | $2.9^{+0.2}_{-0.3}$ | $4.5^{+0.2}_{-0.3}$ | $0.86^{+0.07}_{-0.1}$ | $1.44^{+0.09}_{-0.1}$ | 2.4 ± 0.2 |
| CL 1040.7–1155 | 0.7043 | $R - I$ | $0.05^{+0.02}_{-0.01}$ | $1.1^{+0.4}_{-0.7}$ | $3.2^{+0.3}_{-0.6}$ | $4.9^{+0.2}_{-0.4}$ | 0.9 ± 0.1 | 1.6 ± 0.2 | $2.7^{+0.2}_{-0.3}$ |
| CL 1054.7–1245a | 0.7305 | $R - I$ | $0.11^{+0.06}_{-0.02}$ | $0.5^{+0.5}_{-0.4}$ | $1.6^{+0.5}_{-1}$ | $4.0^{+0.2}_{-0.5}$ | $0.80^{+0.1}_{-0.07}$ | $1.4^{+0.1}_{-0.2}$ | $2.1^{+0.1}_{-0.3}$ |
| CL 1054.7–1245 | 0.7498 | $R - I$ | $0.10^{+0.02}_{-0.01}$ | $0.6^{+0.3}_{-0.4}$ | $1.8^{+0.3}_{-0.4}$ | $3.6^{+0.1}_{-0.2}$ | $0.84^{+0.06}_{-0.08}$ | $1.30^{+0.08}_{-0.11}$ | $1.90^{+0.06}_{-0.1}$ |
| CL 1354.2–1230 | 0.7620 | $R - I$ | $0.05^{+0.03}_{-0.01}$ | $0.9^{+0.5}_{-0.8}$ | $2.9^{+0.4}_{-0.9}$ | $4.6^{+0.3}_{-0.7}$ | $0.9^{+0.1}_{-0.2}$ | $1.6^{+0.2}_{-0.4}$ | $2.7^{+0.3}_{-0.5}$ |
| CL 1216.8–1201 | 0.7943 | $R - I$ | $0.058^{+0.009}_{-0.006}$ | $0.9^{+0.2}_{-0.3}$ | $2.8^{+0.2}_{-0.2}$ | $4.5^{+0.1}_{-0.2}$ | $0.96^{+0.05}_{-0.07}$ | 1.6 ± 0.1 | $2.75^{+0.09}_{-0.2}$ |

(or cluster mass). This method has been used by many authors in the past (e.g. Stanford et al. 1998; van Dokkum et al. 1998; Blakeslee et al. 2003, 2006; Mei et al. 2006, 2009; Hilton et al. 2009). A description of the specific steps we took to perform the scatter–age test follows.

We first constructed CMDs of the early-type galaxies in each cluster using the photometric bands closest to rest-frame U and V . Rest-frame $U - V$ measures the strength of the 4000 Å break and is therefore a very age-sensitive broad-band colour (see Section 3.1 for a detailed justification of our choice of observed colour). For most of the clusters this choice required CMDs of $R - I$ versus I , but for the three lowest redshift clusters we used $V - I$ versus I (see Table 2). We then fitted a linear CMR for each cluster using a fixed slope of -0.09^1 and setting the zero-point to the median colour. This procedure is very robust, in particular for groups and clusters with small numbers of galaxies where the CMR slope cannot be determined to sufficient accuracy. Our results are not sensitive to the exact choice of slope since in general the CMR is reasonably flat and redshift independent (Holden et al. 2004). As an example, the CMD for the early-type galaxies in cluster CL 1216.8–1201 is shown in Fig. 2.

For each cluster, the observed scatter in the galaxy colours about the CMR (σ_{obs}) was computed as the rms of the residuals (in the colour direction) between the observed colours and the fitted CMR. We reject outliers in this process by imposing the condition that galaxy colours should be within ± 0.3 mag from the CMR. While other methods such as the biweight scatter estimator used by other authors (e.g. Mei et al. 2009) reject outliers implicitly, we chose to do it explicitly. We discuss these outliers in some detail later.

Following Bower et al. (1992), the intrinsic scatter (σ_{int}) was then obtained by subtracting, in quadrature, the mean value of the photometric colour uncertainty from the observed scatter. The colour uncertainties range from 0.012 to 0.021 (White et al. 2005), and have therefore little effect on the observed scatter (see Section 4).

¹ This value was previously used in De Lucia et al. (2007) to construct $V - I$ CMRs for colour-selected red-sequence galaxies from the EDisCS data base.

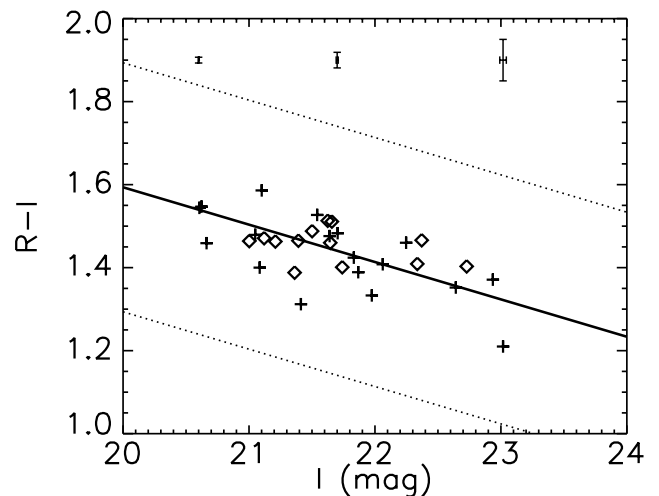


Figure 2. The $R - I$ versus I CMD for the early-type galaxies in cluster CL 1216.8–1201 at $z = 0.79$ is shown here as an example. Elliptical galaxies are represented by ‘+’ signs, and S0s by open diamonds. The solid line shows a linear fit to the CMR with the slope value determined by De Lucia et al. (2007). See text for details. The dotted lines correspond to ± 0.3 mag from the CMR. For reference, the typical sizes of the error bars are plotted on the top of the figure as a function of magnitude.

Bower et al. (1992) used σ_{int} to constrain the formation history of the galaxies by assuming the following relationship between the colour scatter and the colour evolution of the stellar population (Bower et al. 1992):

$$\delta(U - V)_0 = \frac{d(U - V)_0}{dt}(t_{\text{H}} - t_{\text{F}})\beta \leq \sigma_{\text{int}}, \quad (1)$$

where t_{H} is the age of the universe at the cluster redshift, t_{F} is the look-back time from then to the epoch at which star formation ended and $d(U - V)_0/dt$ (where the subscript ‘0’ denotes rest frame) is derived from galaxy evolution models. This factor should be reasonably well understood as it is mainly governed by main-sequence evolution [for a given initial mass function (IMF)]. In this equation, β parametrizes the spread in formation time Δt as a fraction of the

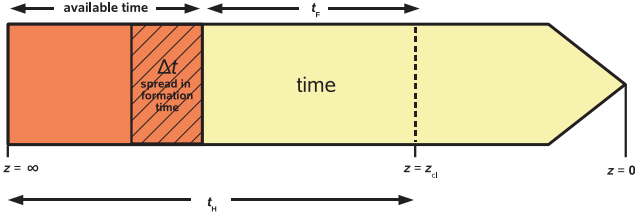


Figure 3. Time-line of the Universe illustrating the different parameters used in equations (1) and (2). The time arrow starts on the left at the beginning of the universe ($z = \infty$). The orange region shows the total available time galaxies can use to form stars. Δt is the time galaxies actually spend forming stars. From then on, the cluster galaxies are assumed to evolve passively until the observed redshift (z_{cl}). We define t_F as the time elapsed from the epoch when star formation ended until the cosmic time corresponding to z_{cl} .

total available time:

$$\beta = \frac{\Delta t}{(t_H - t_F)}. \quad (2)$$

Thus, $\beta = 1$ implies no synchronization, i.e. the galaxies in the sample formed using all the available time, while $\beta = 0.1$ would mean a high degree of synchronization, with all the galaxies forming in the last 10 per cent of the available time. Fig. 3 illustrates the time-line defined by equations (1) and (2).

We calculated the $d(U - V)_0/dt$ factor using Bruzual & Charlot (2003, hereafter BC03) models² for a passively evolving stellar populations that formed in a single burst of 0.1 Gyr duration. The exact burst duration does not have a significant effect on our conclusions provided that it is much shorter than t_F . Solar metallicity ($Z_{\odot} = 0.02$), a Chabrier (2003) IMF and no dust attenuation were assumed. Using alternative IMFs (e.g. Salpeter 1955) would not alter our conclusions because for the stellar masses of interest (given the range in t_F), the relative differences in the IMFs are only minor (cf. Bower et al. 1992). The use of models with solar metallicity is partially motivated by the results presented in Sánchez-Blázquez et al. (2009), where ages and metallicities are derived for EDisCS red-sequence galaxies from their absorption line indices. Sánchez-Blázquez et al. (2009) found solar-metallicity models agreed well with the observed galaxy spectra. We discuss the effect of assuming different metallicities later.

Fig. 4 shows how equation (1) can be used to constrain the star formation history of the galaxies from the colour scatter σ_{int} of our richest cluster. It also illustrates the effect of the relevant random and systematic uncertainties. In Fig. 4(a), the red solid line represents $d(R - I)/dt$ (very close to rest-frame $d(U - V)_0/dt$) as a function of t_F , calculated from the BC03 models. The black solid lines are defined by the equation

$$\frac{d(R - I)}{dt} = \frac{\sigma_{int}}{(t_H - t_F)\beta} \quad (3)$$

for several values of β . Equation (1) implies that the allowed region lies below the black lines, and thus the intersection of the red and black lines provides a constraint (upper limit) on t_F for a given β . It is clear that the colour scatter alone cannot be used to constrain t_F and β simultaneously. The dotted black lines in Fig. 4(a) represent

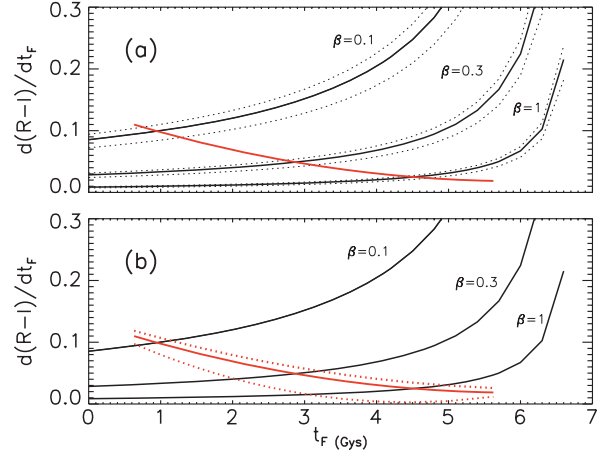


Figure 4. Illustration of the colour-scatter method and the associated random (a) and systematic (b) uncertainties for the cluster CL 1216.8–1201 at $z = 0.79$. The rate of colour change ($d\text{Colour}/dt$) as a function of t_F is shown by the identical solid red lines in panels (a) and (b). In this example we use the observed $(R - I)$, very close to rest-frame $(U - V)$ at the cluster redshift, computed using BC03 stellar population models for galaxies with solar metallicity and a single star formation burst of 0.1 Gyr duration (see text for details). The scatter about the CMR provides an upper limit to the allowed rate of colour evolution, parametrized by equation (3) for a given β (equation 2). This constraint is shown in both panels by the identical solid black lines, as derived from the intrinsic colour scatter for this cluster and assuming three different values of β . The intersection between the observational lines (solid black) and the model ones (solid red) constrains t_F . The dotted black lines in panel (a) correspond to the $\pm 1\sigma$ random errors affecting the solid black line as a result of the observational uncertainty in the colour scatter. The red dotted lines in panel (b) illustrate the effects of systematic model uncertainties (e.g. metallicity) on t_F . These lines correspond to models with the same star formation history as for the red solid line but different metallicities: the upper line has $Z_{\text{substellar}} = 0.008$, whilst the lower line has $Z_{\text{supersolar}} = 0.05$.

the $\pm 1\sigma$ random errors³ in the colour scatter, showing their effect on the t_F uncertainty. The effect of systematic uncertainties, such as changing the model chemical composition, is shown in panel (b). The dotted red lines correspond to stellar population models with non-solar metallicity ($Z_{\text{substellar}} = 0.008$ and $Z_{\text{supersolar}} = 0.05$). It is immediately apparent that the effect of systematic model uncertainties such as these in the calculation of t_F is, in general, significantly larger than that of photometric random errors. This implies that absolute values of t_F must be interpreted with great caution. However, it is not unreasonable to assume that these systematics would affect all the galaxies similarly, making any *differential* or *comparative* study precise and, hopefully, robust. Unless otherwise stated, we consider random uncertainties only when discussing t_F since our study is largely comparative, but it is important to bear in mind that substantial systematic uncertainties do exist.

3.1 Colour dependence of the derived t_F

Previous studies have noted that colours which bracket the 4000 Å break provide the most sensitive indicators of age changes, yet the least affected by photometric errors (e.g. Blakeslee et al. 2006). For this reason, and following Bower et al. (1992), we decided to

² For the range of ages discussed in this paper and the optical colours on which we base our conclusions, using alternative population synthesis models such as those of Maraston (2005) would not change our results.

³ The errors in the colour scatter were estimated from the 16 and 84 per cent confidence levels in the χ^2 distribution of the measured σ_{int} , which correspond to $\pm 1\sigma$ uncertainties.

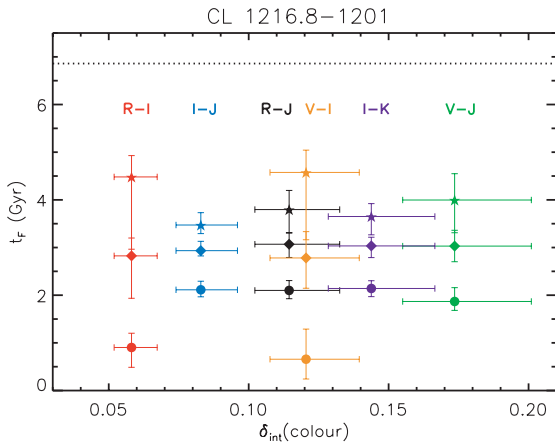


Figure 5. The derived formation times of the early-type galaxies in the cluster CL 1216.9–1201 at $z = 0.79$ are plotted against the intrinsic CMR scatter measured for the different colours used in the scatter analysis. With the exception of $I - J$ and $I - K$ all colours straddle the 4000 \AA break at the cluster redshift. Filled stars correspond to $\beta = 1.0$, diamonds to $\beta = 0.3$ and circles to $\beta = 0.1$ (see equation 2). The black dotted line indicates the age of the Universe (t_H) at the cluster redshift. In this figure the errors in t_F are calculated as the sum (in quadrature) of the random and systematic uncertainties discussed in the text. Within the errors, most colours yield consistent values of t_F (particularly for $\beta \geq 0.3$). However, for $\beta = 0.1$ the optical–optical and optical–IR colours give discrepant results possibly due to the difficulty in modelling the contribution of asymptotic giant branch stars.

carry out the age-scatter test using observed colours close to rest-frame $U - V$. Nevertheless, it is instructive to study how the actual colour choice could affect our results. We used our richest cluster, CL 1216.8–1201, as the ideal test bed for this purpose. Using the galaxy sample in this cluster, we carried out the scatter–age test with CMDs compiled for different sets of colours. Most colours straddle the 4000 \AA break at $z = 0.79$ (the cluster redshift), with the exceptions of $I - J$ and $I - K$. The values of σ_{int} and t_F derived for each colour are plotted in Fig. 5 for different values of β . It is clear that, at least for $\beta \geq 0.3$, all the colours provide a consistent value of t_F within the combined random and systematic errors. However, for $\beta = 0.1$ the optical–optical and optical–infrared colours give discrepant results. This is probably because at the relevant stellar population ages (1–2 Gyr) asymptotic giant branch stars have a potentially large, and very uncertain, contribution to the near-IR galaxy emission, making the model predictions very unreliable (Maraston 2005; Conroy & Gunn 2010). The colour with the smallest scatter and smallest scatter uncertainty is $R - I$, which is the closest to rest-frame $U - V$ at this redshift. This provides additional justification for the use of observed colours that are the closest match to rest-frame $U - V$ in our analysis.

4 THE SCATTER IN THE COLOUR–MAGNITUDE RELATION

4.1 The CMR scatter for different clusters

For each cluster, we calculated the intrinsic colour scatter σ_{int} following the method described in Section 3. The values of σ_{int} and the actual colours used for each cluster are listed in Table 2. At this stage, we exclude from this calculation all galaxies whose colours are >0.3 mag bluer than the fitted CMR. The number of galaxies

excluded in each cluster is listed in Table 1. In total, there are 12 (7 per cent) of these blue early-type galaxies in our sample. We justify this approach and discuss these galaxies later.

The colour scatter shows no significant evolution with redshift for the clusters in the EDisCS sample (Fig. 6, top panel). To extend the redshift baseline and compare our results with previous studies, we plot in Fig. 6 similar colour scatter measurements from the sources listed in Table 3. No redshift dependence is found even for this extended redshift range. The bottom panel of Fig. 6 further shows that the colour scatter does not correlate with cluster velocity dispersion (σ_v) either, implying that the scatter is not strongly affected by cluster mass. We note that the velocity dispersion range spanned by our sample is very broad ($200 \lesssim \sigma_v \lesssim 1200 \text{ km s}^{-1}$). Adding the clusters in the comparison samples reinforces our result.

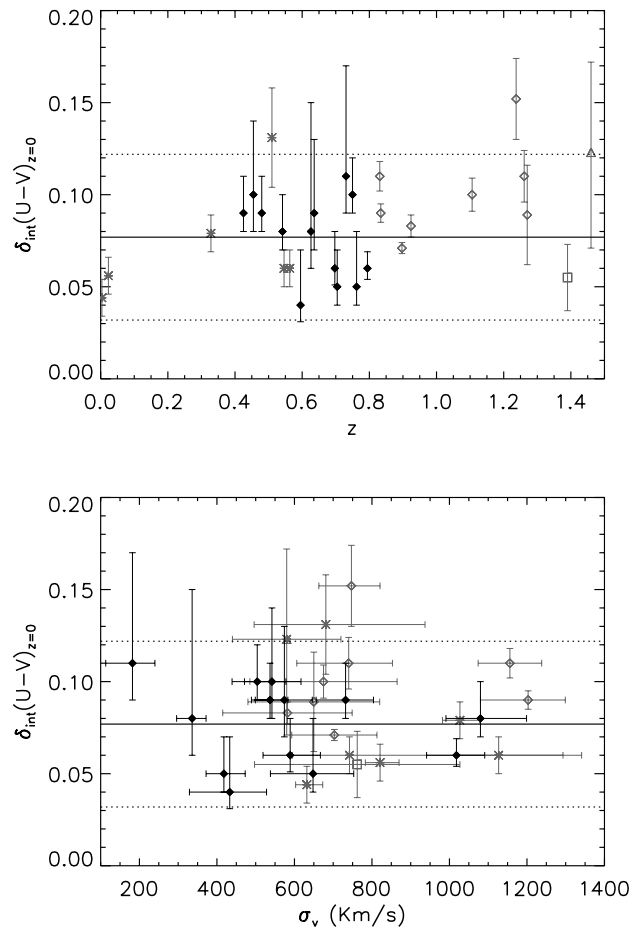


Figure 6. The upper panel shows the dependence of the intrinsic scatter in the observed colour closest to rest-frame $(U - V)_{z=0}$ for EDisCS clusters (filled black diamonds) and several comparison samples at lower and higher redshift (grey symbols). The low-redshift cluster sample (asterisks) was compiled from the work of Bower et al. (1992), van Dokkum et al. (1998) and Ellis et al. (1997). The higher redshift sample was taken from Mei et al. (2009) (open diamonds), Hilton et al. (2009) (open triangle) and Lidman et al. (2008) (open square). See Table 3 for details about the comparison samples. This plot reveals there is no significant CMR scatter evolution with redshift up to $z < 1.5$. The lower panel shows the scatter as function of cluster velocity dispersion. In both panels, the solid line represents the median σ_{int} value for the EDisCS clusters and the dotted lines correspond to $\pm 2\sigma$. The CMR scatter does not correlate with cluster velocity dispersion.

Table 3. Main characteristics of the comparison samples.

| | Cluster name | z | σ_{int} | Colour used in σ_{int} | Ref. for σ_{int} | σ_v (km s^{-1}) | Ref. for σ_v | Symbols in Fig. 6 |
|---------------|---------------------|--------|-----------------------|---|-----------------------------------|--------------------------------------|------------------------|----------------------|
| Low z | Coma | 0.0231 | 0.056 ± 0.01 | $U - V$ | 1 | 821^{+49}_{-38} | 8 | * |
| | Virgo | 0.0038 | 0.044 ± 0.01 | $U - V$ | 1 | 632^{+41}_{-29} | 8 | * |
| | CL 1358+62 | 0.3283 | 0.079 ± 0.01 | $B - V$ | 2 | 1027^{+51}_{-45} | 9 | * |
| | CL 0412-65 | 0.510 | 0.131 ± 0.027 | $(U - V)_{z=0}$ | 3 | 681^{+256}_{-185} | 10 | * |
| | CL 0016+16 | 0.546 | 0.06 ± 0.01 | $(U - V)_{z=0}$ | 3 | 1127^{+166}_{-112} | 7 | * |
| | CL 0054-27 | 0.563 | 0.06 ± 0.01 | $(U - V)_{z=0}$ | 3 | 742^{+599}_{-147} | 10 | * |
| High z | MS 1054-0321 | 0.831 | 0.070 ± 0.008 | $(U - B)_{z=0}$ | 4 | 1156 ± 82 | 4 | ◇ |
| | RX J0152.7-1357 | 0.834 | 0.050 ± 0.005 | $(U - B)_{z=0}$ | 4 | 1203^{+96}_{-123} | 4 | ◇ |
| | CL 1604+4304 | 0.897 | 0.031 ± 0.003 | $(U - B)_{z=0}$ | 4 | 703 ± 110 | 4 | ◇ |
| | CL 1604+4321 | 0.924 | 0.043 ± 0.006 | $(U - B)_{z=0}$ | 4 | 582 ± 167 | 4 | ◇ |
| | RDCS J0910+5422 | 1.106 | 0.060 ± 0.009 | $(U - B)_{z=0}$ | 4 | 675 ± 190 | 4 | ◇ |
| | RDCS J1252.9-2927 | 1.237 | 0.112 ± 0.022 | $(U - B)_{z=0}$ | 4 | 747^{+74}_{-84} | 4 | ◇ |
| Very high z | RX J0849+4452 | 1.261 | 0.070 ± 0.014 | $(U - B)_{z=0}$ | 4 | 740^{+113}_{-134} | 4 | ◇ |
| | RX J0848+4453 | 1.270 | 0.049 ± 0.027 | $(U - B)_{z=0}$ | 4 | 650 ± 170 | 4 | ◇ |
| | XMMU J2235.3-2557 | 1.39 | 0.055 ± 0.018 | $J - K_s$ | 5 | 762 ± 265 | 11 | □ |
| | XMMXCS J2215.9-1738 | 1.46 | 0.12 ± 0.05 | $z_{850} - J$ | 6 | 580 ± 140 | 11 | △ |

Note. Following Blakeslee et al. (2006), the scatter in $(U - B)_{z=0}$ was transformed into $(U - V)_{z=0}$ scatter by adding 0.04.

References: 1 – Bower et al. (1992); 2 – van Dokkum et al. (1998); 3 – Ellis et al. (1997); 4 – Mei et al. (2009) and references therein; 5 – Lidman et al. (2008); 6 – Hilton et al. (2009); 7 – Borgani et al. (1999); 8 – Fadda et al. (1996); 9 – Fisher et al. (1998); 10 – Girardi & Mezzetti (2001); 11 – Mullis et al. (2005); 12 – Hilton et al. (2007).

4.2 CMR scatter dependence on galaxy properties

To explore the overall behaviour of the galaxy colours around the CMR, Fig. 7 shows the distribution of the residuals for the complete galaxy sample as a function of the absolute rest-frame B magnitude M_B (for details of the calculation of M_B , see Rudnick et al. 2009). By construction, the residuals are concentrated about their median value (≈ 0 ; solid line in Fig. 7). The vast majority of the colour residuals follow a normal distribution reasonably well. The scatter is small, as discussed above. However, at faint magnitudes there is a clear ‘blue-tail’ containing a few galaxies with significantly bluer colours (smaller blue symbols in Fig. 7). These results can also be seen in the upper histogram of Fig. 8, which shows the

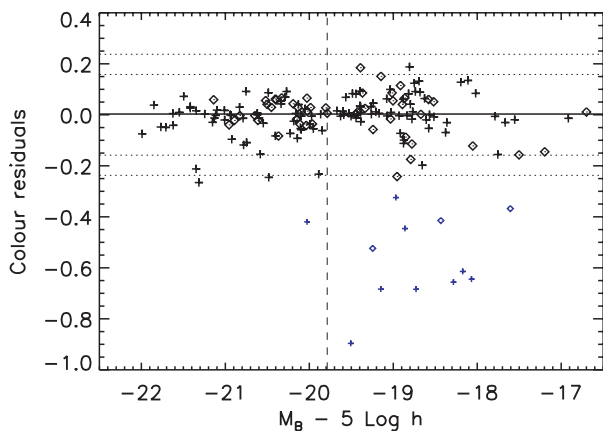


Figure 7. Observed colour residuals around the CMR as a function of M_B of all the galaxies in the sample. Note that we express the magnitude as $M_B - 5 \log h$, where $h = H_0/70$. Elliptical galaxies are represented with crosses and lenticulars with diamonds. The solid line indicates the location of the median, dotted lines correspond to 2σ and 3σ for the black data points and the blue symbols represent the galaxies in the ‘blue tail’ (see text for details). The median luminosity is also shown for reference (black dashed line).

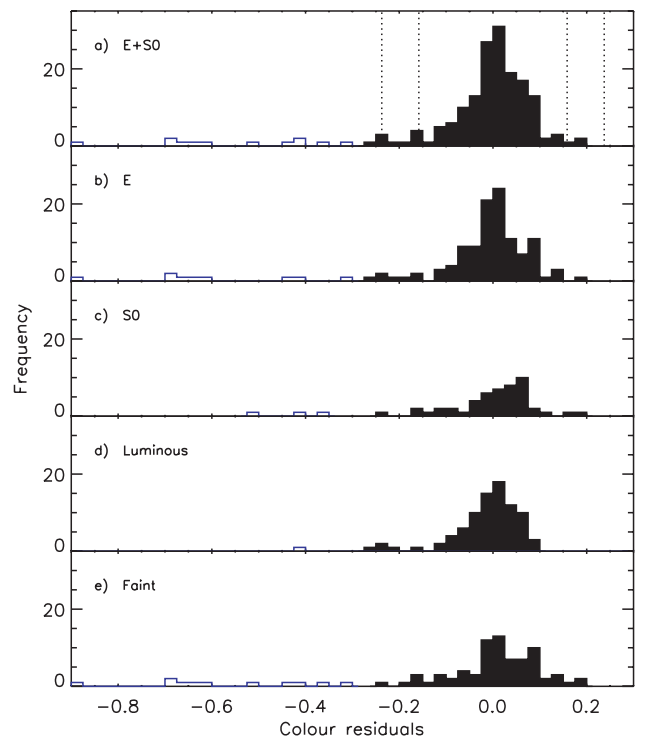


Figure 8. Histograms of the observed colour residuals around the CMR for the different galaxy subsamples computed from Fig. 7: (a) the complete sample (Ellipticals and S0s); (b) ellipticals only; (c) S0s only; (d) luminous galaxies and (e) faint galaxies. The dotted lines in the top panel correspond to 2σ and 3σ for a Gaussian distribution with $\sigma_{\text{obs}} = 0.078$. The open blue part of each histogram corresponds to the ‘blue tail’ (see text and Fig. 7 for details).

Table 4. Properties of the ‘blue tail’ galaxies. The ‘excluded’ galaxies are also listed in the two bottom lines.

| EDisCS galaxy ID | Type | Residual (mag) | M_B | Comments (from spectra; morphology) |
|------------------------|----------|----------------|--------|--|
| EDCSN J1054199–1146065 | E | −0.32 | −18.97 | Several emission lines |
| EDCSN J1054207–1148130 | S0 | −0.41 | −18.43 | Considerable [O II] emission |
| EDCSN J1232307–1249573 | E | −0.90 | −19.51 | Absorption-line spectra |
| EDCSN J1232336–1252103 | S0 | −0.52 | −19.24 | Galaxy of spectral type k+a |
| EDCSN J1232304–1250391 | E | −0.42 | −20.03 | Considerable [O II] emission; some sign of disturbance |
| EDCSN J1138050–1132546 | E | −0.60 | −18.17 | Strong [O II] emission |
| EDCSN J1138068–1132510 | E | −0.68 | −18.73 | Starburst?: high surface brightness |
| EDCSN J1138034–1133049 | E | −0.64 | −18.07 | Strong [O II] emission; some sign of disturbance |
| EDCSN J1354073–1233336 | E | −0.45 | −18.86 | Strong [O II] emission |
| EDCSN J1354022–1234283 | E | −0.68 | −19.15 | Strong [O II] emission; compact galaxy |
| EDCSN J1037564–1245134 | S0 | −0.37 | −17.61 | Considerable [O II] emission |
| EDCSN J1138135–1137137 | E | −0.66 | −18.28 | Considerable [O II] emission |
| EDCSN J1138096–1135223 | <i>a</i> | −0.33 | −19.00 | Strong [O II] emission; very disturbed/merging |
| EDCSN J1138127–1134190 | <i>a</i> | −0.33 | −17.88 | Either H II regions or large merger |

^aThese galaxies were misclassified as E in Desai et al. (2007). We excluded them from the sample since their *HST* images reveal that they are not early-type galaxies and they show strong signs of disruption (see Section 2).

Table 5. Scatter analysis results for the morphology and luminosity-split subsamples. The colour scatter and the derived formation times and redshifts are given for three values of β .

| Sample | $\langle z \rangle$ | σ_{int} | $t_F(\beta = 0.1)$ | $t_F(\beta = 0.3)$ | $t_F(\beta = 1.0)$ | $z_F(\beta = 0.1)$ | $z_F(\beta = 0.3)$ | $z_F(\beta = 1.0)$ |
|----------|---------------------|---------------------------|------------------------|------------------------|------------------------|------------------------|------------------------|------------------------|
| All | 0.6411 | $0.077^{+0.005}_{-0.004}$ | $2.64^{+0.07}_{-0.08}$ | $4.04^{+0.06}_{-0.07}$ | $5.45^{+0.06}_{-0.07}$ | $1.22^{+0.3}_{-0.3}$ | $1.85^{+0.04}_{-0.05}$ | $2.88^{+0.07}_{-0.08}$ |
| E | 0.6443 | $0.075^{+0.005}_{-0.004}$ | $2.65^{+0.09}_{-0.1}$ | $4.05^{+0.08}_{-0.09}$ | $5.45^{+0.07}_{-0.09}$ | $1.22^{+0.3}_{-0.3}$ | $1.85^{+0.04}_{-0.05}$ | $2.88^{+0.07}_{-0.08}$ |
| S0 | 0.6589 | $0.079^{+0.009}_{-0.007}$ | $2.6^{+0.1}_{-0.2}$ | $4.0^{+0.1}_{-0.1}$ | $5.3^{+0.1}_{-0.1}$ | $1.24^{+0.05}_{-0.05}$ | $1.87^{+0.06}_{-0.07}$ | $2.9^{+0.1}_{-0.1}$ |
| Luminous | 0.7016 | $0.070^{+0.006}_{-0.005}$ | 2.636 ± 0.1 | $4.00^{+0.08}_{-0.1}$ | $5.33^{+0.08}_{-0.09}$ | $1.34^{+0.04}_{-0.05}$ | $2.03^{+0.08}_{-0.09}$ | $3.1^{+0.2}_{-0.2}$ |
| Faint | 0.6071 | $0.080^{+0.007}_{-0.006}$ | $2.668^{+0.1}_{-0.1}$ | $4.10^{+0.09}_{-0.1}$ | $5.6^{+0.1}_{-0.1}$ | $1.11^{+0.03}_{-0.04}$ | $1.67^{+0.05}_{-0.05}$ | $2.65^{+0.08}_{-0.09}$ |

distribution of the colour residuals for the complete sample of early-type cluster galaxies. The measured scatter for the whole sample is small ($\sigma_{\text{obs}} = 0.078$ when excluding the ‘blue-tail’) and significantly larger than the scatter due to the photometric errors ($\simeq 0.017$). This implies that the intrinsic colour scatter for the complete sample is $\sigma_{\text{int}} = 0.076^{+0.005}_{-0.004}$, very close to the average scatter for the individual clusters ($\langle \sigma_{\text{int}} \rangle = 0.077$, cf. Table 2).

There are 12 galaxies (7 per cent of the total sample) with colours > 0.3 mag bluer than the CMR. The number of ‘blue’ galaxies in each cluster is listed in Table 1, while their individual IDs and some observed properties are presented in Table 4. These galaxies were excluded from our scatter–age analysis (Section 5) for consistency with previous studies (e.g. Mei et al. 2009) where outliers are rejected implicitly. We prefer to exclude them explicitly but discuss the implications that their existence and properties have in our conclusion. Interestingly, two out of the 12 blue galaxies show a small degree of disruption in their morphologies, as found by visually inspecting their *HST* images (see comments in Table 4 and Fig. 1). In Section 2 we found six galaxies (4 per cent) in our full sample that, despite their clear early-type morphology, show some signs of disruption. Now we find that two of these disturbed galaxies have ‘blue’ colours, indicating that among the blue galaxies, morphological disturbances are much more common than among the ones in the CMR. Nevertheless, the rest of the blue galaxies (10) do not show any clear sign of morphological disruption. We further discuss the implications of these faint blue galaxies (i.e. the ‘blue tail’) in our conclusions.

In what follows, we concentrate on the remaining 160 galaxies whose colours are within ± 0.3 mag from the CMR. From these, we constructed subsamples according to different galaxy properties.

(i) Morphology (E versus S0), as indicated by different symbols in Fig. 7.

(ii) Luminosity (luminous versus faint), divided at the median rest-frame B absolute luminosity (corresponding to $M_B^{\text{med}} = -19.8$; cf. vertical dashed line in Fig. 7).

The four bottom histograms of Fig. 8 show the distribution of the colour residuals for each one of these subsamples. Within the errors, we find that both ellipticals and S0s show the same scatter. However, the luminous galaxies have a slightly smaller intrinsic scatter than the faint ones. The values of σ_{int} for each subsample are listed in Table 5. In the next section, we interpret these scatters in terms of the star formation history of the different galaxy samples.

5 STAR FORMATION HISTORIES

5.1 Star formation histories of the early-type galaxies in each cluster

Using the method discussed in Section 3 and the intrinsic colour scatter measured for the early-type galaxies, we computed, for three values of β , the formation times t_F and their respective errors for each individual cluster or group (see Table 2). An inspection of this table immediately shows that, as expected, for higher values of β (less synchronous galaxy formation) older ages are required to explain the small colour scatter. A clear trend is also apparent: at a fixed β , higher redshift clusters have smaller t_F . However, if we correct for the difference in look-back time using our adopted cosmology, these t_F can be translated into formation redshifts, z_F , and the trend disappears. All the EDisCS clusters yield consistent

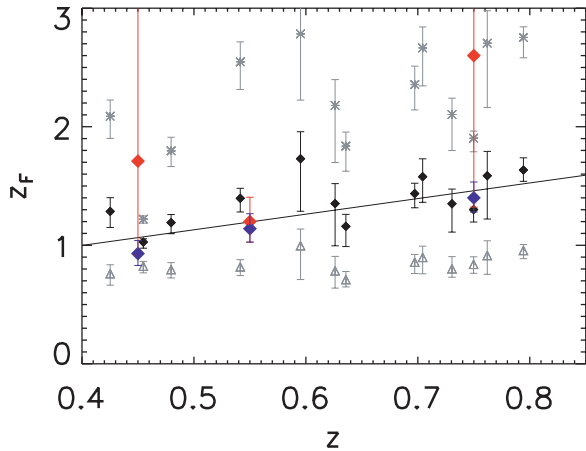


Figure 9. Galaxy formation redshift z_F versus cluster redshift. Symbols correspond to the different values of β used: triangles for $\beta = 0.1$, filled diamonds for $\beta = 0.3$ and stars for $\beta = 1.0$. The solid line is a linear fit to the solid black diamonds. For comparison, the predicted z_F from Sánchez-Blázquez et al. (2009) are shown as larger coloured symbols. The blue diamonds correspond to the morphologically selected sample of EDisCS early-type galaxies with galaxy velocity dispersions $< 175 \text{ km s}^{-1}$, while the red symbols correspond to the sample with galaxy velocity dispersions $> 175 \text{ km s}^{-1}$. The blue points agree very well with our z_F for $\beta = 0.3$, whilst the red points are in agreement with our results if $\beta \geq 0.3$. We observe an increase of z_F with cluster redshift (see also Fig. 10).

formation redshifts for their early-type galaxy population ($z_F \simeq 0.8$ for $\beta = 0.1$, $z_F \simeq 1.4$ for $\beta = 0.3$ and $z_F \simeq 2.4$ for $\beta = 1.0$). This is shown in Fig. 9, where z_F is plotted versus cluster redshift for the different values on β . For comparison, we overplot the formation redshifts derived by Sánchez-Blázquez et al. (2009) using absorption-line indices in the spectra of EDisCS early-type red-sequence galaxies (blue and red diamonds). The blue points (corresponding to galaxies with velocity dispersions $< 175 \text{ km s}^{-1}$) agree very well with our formation redshifts for $\beta = 0.3$ (black diamonds), while the red points (galaxy velocity dispersions $> 175 \text{ km s}^{-1}$) agree with $\beta \geq 0.3$. Moreover, galaxy ages derived from the analysis of the Fundamental Plane of these galaxies (Saglia et al., in preparation) are also in agreement with our formation redshifts for $\beta \geq 0.3$.

Fig. 9 also shows that z_F may be slightly higher for higher redshift EDisCS clusters (fitted line). Although this trend is not very significant, it would be desirable to extend the redshift baseline to test whether it continues at higher redshifts. We can do that by using the study published by Mei et al. (2009). These authors follow a very similar procedure to ours, and predict formation times based on a colour-scatter analysis for a value of $\beta \simeq 0.3$. Their galaxy samples also contain morphologically classified ellipticals and S0s, and can therefore be compared to ours. Their results are plotted as open diamonds in Fig. 10, together with our results for $\beta = 0.3$. If we take these points at face value, the trend of increasing z_F with redshift becomes very significant. However, a word of caution is required. Although our study and that of Mei et al. (2009) are very similar, there are some differences. First, their photometry and the colours that they use are different because the higher redshift of their clusters. Second, they estimate the intrinsic colour scatter using biweight scale estimator (which implicitly excludes outliers). However, using their method with our data does not change our results since we exclude outliers explicitly, as discussed in Section 3. Finally, their implementation of the scatter-age test differs in some minor details from ours, although they use the same BC03 models. We believe these differences are probably not important for this

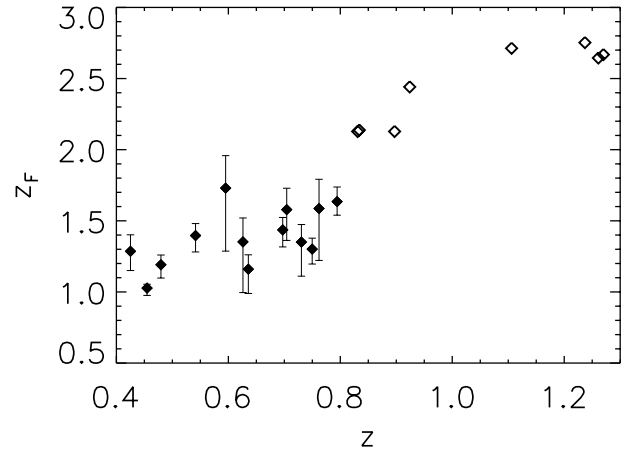


Figure 10. Galaxy formation redshift z_F (derived using $\beta = 0.3$) versus cluster redshift for EDisCS clusters (solid diamonds) and for the clusters published by Mei et al. (2009) (open diamonds). We observe that z_F increases slightly with cluster redshift for the EDisCS sample (see also fitted line in Fig. 9). This trend becomes stronger when we include the higher redshift comparison sample.

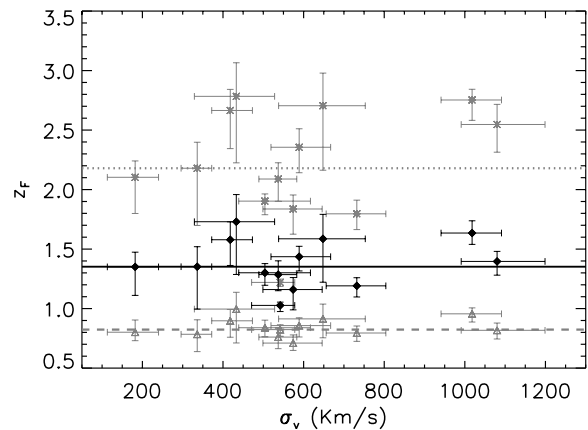


Figure 11. Galaxy formation redshift z_F versus cluster velocity dispersion. As in Fig. 9, symbols correspond to the different values of β : triangles for $\beta = 0.1$, filled diamonds for $\beta = 0.3$ and stars for $\beta = 1.0$. The dashed, solid and dotted lines correspond to the median formation redshift for each value of β . We find that z_F does not depend on the cluster velocity dispersion.

exercise, but we cannot be completely certain without re-analysing their data. With all these caveats, the trend observed in Fig. 10 would imply that that morphologically classified elliptical and S0 galaxies formed earlier in higher redshift clusters than in lower redshift ones.

Fig. 11 shows z_F plotted against cluster velocity dispersion. Consistent with Fig. 6, no correlation is found between z_F and σ_v , implying that the formation time of morphologically classified ellipticals and S0s does not depend strongly on cluster mass.

5.2 Dependence of the star formation histories on galaxy properties

In Table 5, we show the colour scatter and derived formation redshift for the galaxy samples divided in terms of morphology and luminosity, as discussed in Section 4.2. Within the errors, ellipticals and S0s show the same scatter. Since the E and S0 samples have very similar mean redshifts, similar colour scatters imply similar average formation redshift. However, the faint galaxies seem to

exhibit a larger scatter than the bright ones. This, together with the fact that the luminous subsample has a higher average redshift than the faint one, suggests that the most luminous (massive) early-type galaxies formed earlier than the fainter (less massive) ones.

An identical conclusion is reached if the sample is split by stellar mass (derived following Bell & de Jong 2001) instead of by luminosity, which is not surprising since homogeneous colours imply near-constant stellar mass-to-light ratios. When splitting the sample by galaxy velocity dispersion or dynamical mass (cf. Saglia et al., in preparation), similar trends are observed, albeit with smaller statistical significance since only half of the galaxies in our sample have measured velocity dispersions.

6 THE CMR ZERO-POINT

Our CMR scatter analysis cannot constrain t_F and β simultaneously. Until now, we have not discussed the zero-point of the CMR because predicting absolute colours from stellar population models is, arguably, more uncertain than predicting differential colour changes (see e.g. Aragón-Salamanca et al. 1993). However, since accurate zero-points are available, it is worthwhile checking whether consistent and, perhaps, additional constraints can be obtained from them. Fig. 12 shows for each of the EDisCS clusters the CMR colour corresponding to the median absolute B magnitude of the sample, after correcting for luminosity evolution. Specifically, for each cluster we determine the colour of its CMR for $M_B = M_B^* + 1.15$, where M_B^* is empirically determined (Crawford, Bershady & Hoessel 2009; Rudnick et al. 2009). These zero-points do not correlate with intrinsic cluster properties such as their velocity dispersions or masses.

The solid lines in the figure show the predictions of BC03 models for $z_F \sim 1.5$ (corresponding to $\beta = 0.3$, cf. Section 5.1) for $Z_{\text{subsolar}} = 0.008$ (blue), $Z_{\text{solar}} = 0.02$ (black) and $Z_{\text{supersolar}} = 0.05$ (red). It is clear that for median luminosity galaxies non-solar models do not provide an acceptable fit to the galaxy colours for any value

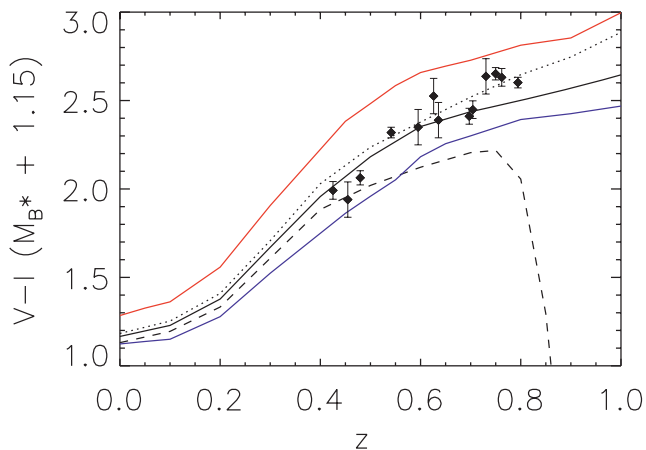


Figure 12. $V - I$ CMR zero-point versus redshift for the EDisCS cluster galaxies (points) compared with population synthesis models from BC03. The black lines have been computed with $Z_{\text{solar}} = 0.02$ metallicity, the blue one with $Z_{\text{subsolar}} = 0.008$ and the red one with $Z_{\text{supersolar}} = 0.05$. The black dashed line corresponds to $\beta = 0.1$ ($z_F \sim 0.9$), the black, blue and red solid lines to $\beta = 0.3$ ($z_F \sim 1.5$) and the black dotted line to $\beta = 1.0$ ($z_F \sim 2.5$). See text for details. The observed points clearly rule out a $\beta = 0.1$ scenario (i.e. very synchronized formation for all the galaxies). However, they are in agreement with $\beta \geq 0.3$.

of β .⁴ However, solar-metallicity models do a reasonable job. This provides additional justification for the use of solar-metallicity models in our analysis (cf. Section 3).

Taking the solar models at face value, a constraint on β can be derived from Fig. 12. The black-dashed line corresponds to $\beta = 0.1$ ($z_F \sim 0.9$), the black solid line to $\beta = 0.3$ ($z_F \sim 1.5$) and the black dotted line to $\beta = 1.0$ ($z_F \sim 2.5$). The observed points clearly rule out $\beta = 0.1$ (i.e. very synchronized formation for all the galaxies). They are in reasonably good agreement with $\beta = 1.0$, but $\beta = 0.3$ is not ruled out. Hence, it seems reasonably safe to conclude that $\beta \geq 0.3$ on the basis of this analysis. If we translate this into the time interval Δt over which all the galaxies ‘formed’, the constraint translates to $\Delta t \gtrsim 1$ Gyr. Since t_F refers to the time at which star formation ceased, this implies that there was an extended epoch over which cluster galaxies had their star formation truncated/stopped. In other words, this cessation of star formation was not synchronized for all the cluster early-type galaxies.

7 DISCUSSION AND CONCLUSIONS

In this paper, we have studied the CMR for a sample of early-type galaxies from the EDisCS. Our sample consists of 172 strictly morphologically classified ellipticals and S0 galaxies in 13 clusters and groups with redshifts $0.4 < z < 0.8$ and velocity dispersions $200 \lesssim \sigma_v \lesssim 1200$ km s⁻¹. All these galaxies are spectroscopically confirmed cluster members, and their magnitudes span the range $-22 \lesssim M_B - 5 \log h \lesssim -17.5$. We have analysed the colour scatter about the CMR and its zero-point to derive meaningful constraints on the formation history of these galaxies. Assuming that the intrinsic colour scatter about the CMR is due to differences in stellar population ages, our main results are as follows.

(i) In agreement with previous studies, the intrinsic colour scatter σ_{int} about the CMR in rest-frame $U - V$ is small ($\sigma_{\text{int}} = 0.076$). However, there is a small minority of faint early-type galaxies (7 per cent) that are significantly bluer than the CMR and were excluded from the scatter analysis. These galaxies probably represent a population of young galaxies that have not yet joined the red-sequence population. Interestingly, only two out of the 12 blue galaxies show signs of morphological disturbances and/or interactions, while the rest are bona-fide ellipticals or S0s. However, the vast majority of the blue galaxies have emission lines in their spectra indicative of ongoing star formation (see Table 4). Faint blue low-mass early-type galaxies have been reported in previous studies (e.g. Blakeslee et al. 2006; Bamford et al. 2009), preferentially in low-density environments. To explain the existence of these low-mass blue early-type galaxies with normal E/S0 morphologies in the field, Huertas-Company et al. (2010) and Kannappan, Guie & Baker (2009) propose two possible explanations. First, they could be the result of minor mergers, which would trigger centrally concentrated star formation, helping to build a bulge, and eventually taking them to the red sequence. Alternatively, the discs in these galaxies are perhaps being (re)built from the surrounding gas, moving then back (or staying) in the blue cloud. It is hard to see how this second possibility would work in the cluster environment, where it is more likely that gas is removed than allowed to fall on to these low-mass galaxies. In clusters, minor mergers remain a possibility, in particular if they occur while these galaxies were in filaments and/or groups, but they need to be minor enough to avoid strong

⁴ For clarity, we show the non-solar metallicity lines for $\beta = 0.3$ only.

morphological disruption. It is also possible that these galaxies are just approaching the cluster for the first time, and will eventually stop forming stars due to gas removal by the cluster environment. This would take them to the red sequence without severely disrupting their morphologies.

(ii) We observe no significant evolution of the intrinsic colour scatter to $z \simeq 0.8$ from the EDisCS clusters alone. This result is consistent with previous studies (e.g. Ellis et al. 1997). After expanding our sample with higher redshift clusters from the literature, we have still found no significant evolution in σ_{int} up to $z \sim 1.5$. Moreover, in the wide range of cluster velocity dispersion (mass) of our sample ($100 \lesssim \sigma_v \lesssim 1300$) the scatter does not seem to show any trend. Because our sample is strictly morphologically selected, this implies that by the time cluster elliptical and S0 galaxies achieve their morphology, the vast majority have already joined the red sequence. The only exception seems to be the very small fraction ($\lesssim 7$ per cent) of faint blue early types.

(iii) Following the work of Bower et al. (1992), we used the colour scatter to estimate the galaxies' formation time t_F , defined as the time elapsed since the major episode of star formation. This allowed us to calculate the formation redshift z_F for the early-type galaxy population in each cluster. Yet again, we measured no significant dependency of z_F on the cluster velocity dispersion. However, we found that z_F increases weakly with cluster redshift within the EDisCS sample. This trend becomes very clear when the higher redshift clusters from Mei et al. (2009) are included. This implies that, at any given redshift, to have a population of fully formed ellipticals and S0s they must have formed most of their stars $\simeq 2$ – 4 Gyr prior to observation. That does not mean that *all* early-type galaxies in *all* clusters formed at these high redshifts. It means that the ones that we observe to already have early-type morphologies also have reasonably old stellar populations. This is partly a manifestation of the 'progenitor bias' (van Dokkum & Franx 1996), but also a consequence of the vast majority of the early-type galaxies in clusters (in particular the massive ones) being already red (i.e. already having old stellar populations) by the time they achieved their morphology.

(iv) Elliptical and S0 galaxies show very similar colour scatter, implying that they have similar stellar population ages. If we assume that their observed properties are representative of the early-type cluster galaxy population at these redshifts, the scarcity of blue S0s indicates that, if they are the descendants of spirals whose star formation has ceased (Aragón-Salamanca, Bedregal & Merrifield 2006; Bedregal, Aragón-Salamanca & Merrifield 2006; Barr et al. 2007), the galaxies were already red when they became S0s, i.e. the parent spiral galaxies became red before losing their spiral arms. The red spirals found preferentially in dense environments (Bamford et al. 2009; Wolf et al. 2009; Masters et al. 2010) are the obvious candidate progenitors of these S0s.

(v) Dividing the sample in two halves by luminosity (or stellar mass), we find that the formation redshift z_F (derived from the CMR scatter in each sample) is smaller for fainter galaxies than for brighter ones. This indicates that fainter early-type galaxies finished forming their stars later. Our results are also consistent with the observation that the cluster red sequence built over time with the brightest galaxies reaching the sequence earlier than fainter ones (De Lucia et al. 2004b, 2007; Rudnick et al. 2009).

(vi) The CMR scatter analysis cannot constrain both the formation time t_F and formation interval Δt simultaneously. However, its combination with the observed evolution of the CMR zero-point, enabled us to conclude that the early-type cluster galaxy population must have had their star formation truncated/stopped over an

extended period $\Delta t \gtrsim 1$ Gyr. Hence, the cessation of star formation was not synchronized for all the cluster early-type galaxies.

ACKNOWLEDGMENTS

Based on observations collected at the European Southern Observatory, Chile, as part of programme 073.A-0216. YLJ acknowledges the European Southern Observatory for financial support and hospitality during the writing of this paper. We also thank Claire Halliday, Bo Milvang-Jensen, Bianca Poggianti and Piero Rosati for useful discussions. GDL acknowledges financial support from the European Research Council under the European Community's Seventh Framework Programme (FP7/2007-2013)/ERC grant agreement no. 202781.

REFERENCES

- Aragón-Salamanca A., Ellis R. S., Couch W. J., Carter D., 1993, MNRAS, 262, 764
 Aragón-Salamanca A., Bedregal A. G., Merrifield M. R., 2006, A&A, 458, 101
 Arimoto N., Yoshii Y., 1987, A&A, 173, 23
 Bamford S. P. et al., 2009, MNRAS, 393, 1324
 Barr J. M., Bedregal A. G., Aragón-Salamanca A., Merrifield M. R., Bamford S. P., 2007, A&A, 470, 173
 Baum W. A., 1959, PASP, 71, 106
 Bedregal A. G., Aragón-Salamanca A., Merrifield M. R., 2006, MNRAS, 373, 1125
 Bell E. F., de Jong R. S., 2001, ApJ, 550, 212
 Bernardi M., Sheth R. K., Nichol R. C., Schneider D. P., Brinkmann J., 2005, AJ, 129, 61
 Blakeslee J. P. et al., 2003, ApJ, 596, L143
 Blakeslee J. P. et al., 2006, ApJ, 644, 30
 Borgani S., Girardi M., Carlberg R. G., Yee H. K. C., Ellingson E., 1999, ApJ, 527, 561
 Bower B., Lucey J., Ellis R., 1992, MNRAS, 254, 601
 Bruzual G., Charlot S., 2003, MNRAS, 344, 1000 (BC03)
 Caldwell N., 1983, AJ, 88, 804
 Chabrier G., 2003, PASP, 115, 763
 Clowe D. et al., 2006, A&A, 451, 395
 Conroy C., Gunn J. E., 2010, ApJ, 712, 833
 Conselice C. J., 2006, MNRAS, 373, 1389
 Crawford S. M., Bershady M. A., Hoessel J. G., 2009, ApJ, 690, 1158
 Dekel A., Silk J., 1986, ApJ, 303, 39
 De Lucia G., Kauffman G., White S. D. M., 2004a, MNRAS, 349, 1101
 De Lucia G. et al., 2004b, ApJ, 610, L77
 De Lucia G. et al., 2007, MNRAS, 374, 809
 De Lucia G., Poggianti B. M., Halliday C., Milvang-Jensen B., Noll S., Smail I., Zaritsky D., 2009, MNRAS, 400, 68
 Desai V. et al., 2007, ApJ, 660, 1151
 Dressler A., 1980, ApJ, 236, 351
 Ellis R., Smail I., Dressler A., Couch W. J., Oemler A., Jr, Butcher H., Sharples R. M., 1997, ApJ, 483, 582
 Faber S. M., 1973, ApJ, 179, 731
 Fadda D., Girardi M., Giuricin G., Mardirossian F., Mezzetti M., 1996, ApJ, 473, 670
 Ferreras I., Charlot S., Silk J., 1999, ApJ, 521, 81
 Finlator K., Davé R., 2008, MNRAS, 385, 2174
 Finn R. A. et al., 2005, ApJ, 630, 206
 Fisher D., Fabricant D., Franx M., van Dokkum P., 1998, ApJ, 498, 195
 Gallazzi A., Charlot S., Brinchmann J., White S. D. M., 2006, MNRAS, 370, 1106
 Girardi M., Mezzetti M., 2001, ApJ, 548, 79
 Gonzalez A. H., Zaritsky D., Dalcanton J. J., Nelson A., 2001, ApJS, 137, 117

- Halliday C. et al., 2004, *A&A*, 427, 397
Hilton M. et al., 2007, *ApJ*, 670, 1000
Hilton M. et al., 2009, *ApJ*, 697, 436
Holden B. P., Stanford S. A., Eisenhardt P., Dickinson M., 2004, *AJ*, 127, 2484
Huertas-Company M., Aguerri J. A. L., Tresse L., Bolzonella M., Koekemoer A. M., Maier C., 2010, *A&A*, 515, 3
Johnson O. et al., 2006, *MNRAS*, 371, 1777
Kannappan S. J., Guie J. M., Baker A. J., 2009, *AJ*, 138, 579
Kauffmann G., Charlot S., 1998, *MNRAS*, 294, 705
Kobayashi C., Springel V., White S. D. M., 2007, *MNRAS*, 376, 1465
Kodama T., Arimoto N., 1997, *A&A*, 320, 41
Kodama T., Arimoto N., Barger A. J., Aragón-Salamanca A., 1998, *A&A*, 334, 99
Larson R. B., 1974, *MNRAS*, 169, 229
Lidman C. et al., 2008, *A&A*, 489, 981
Maraston C., 2005, *MNRAS*, 362, 799
Masters K. L. et al., 2010, *MNRAS*, 405, 783
Mei S. et al., 2006, *ApJ*, 644, 759
Mei S. et al., 2009, *ApJ*, 690, 42
Milvang-Jensen B. et al., 2008, *A&A*, 482, 419
Mullis C. R., Rosati P., Lamer G., Böhringer H., Schwobe A., Schuecker P., Fassbender R., 2005, *ApJ*, 623, 85
Nelán J. E., Smith R. J., Hudson M. J., Wegner G. A., Lucey J. R., Moore S. A. W., Quinney S. J., Suntzeff N. B., 2005, *ApJ*, 632, 137
Pello R. et al., 2009, *A&A*, 508, 1173
Poggianti B. M. et al., 2001, *ApJ*, 563, 118
Poggianti B. M. et al., 2006, *ApJ*, 642, 188
Postman M., Geller M. J., 1984, *ApJ*, 602, 190
Rudnick G. et al., 2009, *ApJ*, 700, 1559
Salpeter E. E., 1955, *ApJ*, 121, 161
Sánchez-Blázquez P. et al., 2009, *A&A*, 499, 47
Sandage A., Visvanathan N., 1978a, *ApJ*, 223, 707
Sandage A., Visvanathan N., 1978b, *ApJ*, 225, 742
Spergel D. N. et al., 2007, *ApJS*, 170, 377
Stanford S. A., Eisenhardt P. R., Dickinson M., 1998, *ApJ*, 492, 461
Tanaka M. et al., 1998, *A&A*, 489, 571
Thomas D., Maraston C., Bender R., Mendes de Oliveira C., 2005, *ApJ*, 621, 673
Trager S. C., Worthey G., Faber S. M., Burstein D., Gonzalez J. J., 1998, *ApJS*, 116, 1
Trager S. C., Faber S. M., Dressler A., 2008, *MNRAS*, 386, 715
Tremonti C. A. et al., 2004, *ApJ*, 613, 898
Treu T. et al., 2005, *ApJ*, 633, 174
Trujillo I., Conselice C. J., Bundy K., Cooper M. C., Eisenhardt P., Ellis R. S., 2007, *MNRAS*, 382, 109
van Dokkum P. G., Franx M., 1996, *MNRAS*, 281, 985
van Dokkum P. G., Franx M., Kelson D. D., Illingworth G. D., Fisher D., Fabricant D., 1998, *ApJ*, 500, 714
van Dokkum P. G., Pieter G., Franx M., Fabricant D., Illingworth G. D., Kelson D. D., 2000, *ApJ*, 541, 95
van Dokkum P. G., Stanford S. A., Holden B. P., Eisenhardt P. R., Dickinson M., Elston R., 2001, *ApJ*, 552, L101
Visvanathan N., Sandage A., 1977, *ApJ*, 216, 214
Wang Y., Yang X., Mo H. J., van den Bosch F. C., 2007, *ApJ*, 664, 608
White S. D. M. et al., 2005, *A&A*, 444, 365
Wolf C. et al., 2009, *MNRAS*, 393, 1302
Worthey G., 1994, *ApJS*, 95, 107

This paper has been typeset from a $\text{\TeX}/\text{\LaTeX}$ file prepared by the author.